# Gust buffeting response of a wind turbine tower in mild and severe wind conditions at Østerild Test Center

# Gust buffeting response of a wind turbine tower in mild and severe wind conditions at Østerild Test Center

Alessandro Giusti*[1b], Tommaso Ballantini[2], Alessio Torrielli[1b] and Claudio Mannini[3a]

[1]*Siemens Gamesa Renewable Energy A/S, Borupvej 16, 7330 Brande, Denmark*
[2]*Department of Civil and Environmental Engineering, University of Florence, Via di Santa Marta 3, 50139 Florence, Italy*
[3]*CRIACIV/Department of Civil and Environmental Engineering, University of Florence, Via di Santa Marta 3, 50139 Florence, Italy*

*(Received keep as blank , Revised keep as blank , Accepted keep as blank )*

**Abstract.** This work focuses on the full-scale gust buffeting response of an isolated wind turbine tower (without rotor-nacelle assembly) about 116 m tall placed at Østerild Test Center (Denmark). It aims to clarify the reliability of analytical models behind design standards through the analysis of combined measurements of wind and structural response. The tower was instrumented with strain gauges mounted close to the base, which indirectly measured the bending moment (net of the mean component), and an accelerometer at about the top. Wind data, mostly velocity and direction at different heights, were recorded by nearby meteorological masts, and they are used to characterize the wind environment in terms of mean velocity profile, turbulence intensity, power spectral density, integral length scale, and coherence of velocity fluctuations. Mild wind conditions, differently from more severe winds, result not well described by the formulations provided by design standards, whereas the coherence function exhibits a disagreement with theoretical models also at high wind velocities. The measured along-wind and across-wind response (in terms of bending moment) is compared with the values got from the direct integration of gust buffeting theory for line-like structures, by using the actual wind characteristics. While a good agreement is found for the along-wind response, especially for the upper bound of the estimated structural damping, the across-wind response significantly deviates from a pure gust buffeting response even at high wind velocity, well above the expected lock-in range. Clear nonlinear aeroelastic response features are highlighted in those cases. Moreover, a comparison with common design standards is developed for the along-wind response, which is significantly underestimated in mild wind conditions.

**Keywords:** gust buffeting; along-wind response; across-wind response; full-scale measurements; mild/severe wind

## 1. Introduction

The dynamic response of finite-length circular cylinders against turbulent wind has recently captured the attention of the wind energy industry. Indeed, towers of wind turbine generators are typically circular cylinders where the rotor-nacelle assembly is mounted on the top. If during the operation of the wind turbine the direct wind-tower interaction has obviously a minor contribution to the overall loads at the base of the tower, this is not true anymore during the different installation stages. Towers, either isolated or in group, can stand for a while without rotor-nacelle assembly during three main moments of the installation process, namely: 1) at the harbor; 2) on the installation vessel (or feeder barge); 3) on the offshore foundation (nowadays mainly monopiles). Harbor quayside operations, also referred to as pre-assembly activities, usually last 6-12 months and primarily consist of storage, transport and lifting of components (tower sections, nacelles, blades), and erection of towers on a freestanding foundation, either full towers or partially assembled towers (sometimes referred to as split towers). The idea is to perform as many operations as possible on land to shorten marine operations, which are one of the main cost drivers (Esteban *et al.*, 2011). At the harbor quayside, towers are usually arranged in groups of $2\times N$ towers (with $N$=2, 3, …, 6), with square mesh and small center-to-center distance. It goes without saying that activities at the harbor quayside are very dynamic, and towers can in principle stand with many different configurations following the permutations of the group. Each tower stays at the harbor around two weeks, i.e., the time between two consecutive load outs of the vessel; afterwards, another tower is erected. Towers are vertically transported on the installation vessel, and they are arranged on the deck with many different group possibilities, similar to those at the quayside, depending on the capabilities of the vessel; for instance, a single tower and a group of four towers are typical configurations. When the vessel reaches the offshore site, the tower is lifted from the grillage of the deck to the foundation, followed by nacelle and blades. It is apparent that a) towers standing without rotor-nacelle assembly at small center-to-center distance are a typical scenario in the wind energy industry, and b) they are associated with temporary stages; c) the latter are usually designed with small return periods, in accordance with the duration of the activities (e.g., see EN 1991-1-6). Moreover, to achieve a safe and cost-effective design, the wind energy industry requires more and more

*Corresponding author
E-mail: alessandro.giusti@siemens-energy.com
[a] Professor
[b] Ph.D.

models able to predict the loads as accurately as possible.

Recent research works dealt with wind turbine towers during those temporary stages, with focus on gust buffeting and vortex shedding response. Mannini *et al.* (2023) assessed by wind tunnel tests the aerodynamic coefficients of several group configurations of wind turbine towers at the harbor quayside, including the effect of helical vortex strakes (Mannini *et al.*, 2024). Moreover, based on a relatively simple gust buffeting model, the inaccuracies in the experimental estimation of the gust factor, due to the effects of imperfect physical modelling in the wind tunnel, were also quantified (Mannini *et al.*, 2026). Full-scale measurements of pressures and structural response on wind turbine towers without rotor-nacelle assembly at Østerild Test Center (Denmark) were used by Kurniawati *et al.* (2024) to investigate the sectional aerodynamic coefficients and vortex shedding loads at transcritical Reynold number regime, together with the analysis of vortex-induced vibrations and post lock-in behavior (Kurniawati *et al.*, 2025). The same experimental data were also processed with operational modal analysis techniques to identify the natural frequencies (Mikkelsen *et al.*, 2024) and the structural damping (Mikkelsen, 2022) of the system.

Besides the abovementioned research works, inspired by actual problems and needs of the wind energy industry, full-scale measurements on chimneys were widely used to study wind-induced vibrations on structures with circular cross-section, starting from the early 1970s. Müller and Nieser (1975) studied a 180 m tall concrete chimney with slenderness (hereafter defined as the ratio of the height to the diameter) from bottom to top in the range 18.26 to 37.89; the properties of excitation and response, and their mutual relationship, were analyzed and compared with theoretical models stressing the role of the cross-correlation. Hirsch and Ruscheweyh (1975) presented the measurements on a 145 m tall steel stack (slenderness of 24.17) equipped with helical vortex strakes, proving the effectiveness of the designed strake system to suppress vibrations; it is noteworthy that the original structure collapsed due to vortex-induced vibrations. Christensen and Askegaard (1978) focused on a 130 m tall concrete chimney with slenderness in the range 7.47 to 22.41 and presented the characterization of the pressure field all around the structure and the related wind-induced vibrations, stressing the dominant oscillation amplitude due to dynamic excitation compared to the static deformation. Hansen (1981) analyzed the same structure during vortex-induced vibrations focusing on the analytical modelling of the response. Melbourne *et al.* (1983), with focus on a 265 m tall reinforced concrete stack with slenderness in the range 12.13 to 21.60, investigated the along- and across-wind response of the structure creating a comprehensive benchmark to be used to validate analytical models. Galemann and Ruscheweyh (1992) studied the wind-induced vibrations of a 28 m tall steel chimney (slenderness of 30.63); the aerodynamic admittance function, along-wind aerodynamic damping, gust factors and across-wind response were compared and discussed against available analytical models. Sanada *et al.* (1992) studied a 200 m tall concrete chimney with slenderness in the range 7.41 to 13.51 during strong typhoons and monsoon events, with focus on pressure field and vortex shedding, providing insights into pressure and force coefficients of the structure. Waldeck (1992) focused on the across-wind response of a 300 m tall concrete chimney and compared analytical predictions with the actual response of the structure, discussing the role of aerodynamic damping. More recently, a chimney (35.5 m tall) was specifically designed to promote vortex-induced vibrations at low wind velocities (Ellingsen *et al.*, 2021); unsteady pressure distributions were studied by using the bi-orthogonal decomposition technique (Manal and Hémon, 2024). Finally, full-scale measurements on chimneys were also used to develop and validate a reliable and robust methodology to reproduce high Reynolds number regimes in wind tunnel tests, for instance through the use of the so-called technical roughness (e.g., Cheng and Kareem, 1992). All these research works stress the importance of full-scale measurements to properly develop and calibrate analytical models. This is also valid for wind turbine towers, which, although they resemble chimneys, have unique peculiarities related to the combination of structural material, geometry (shape, height, and slenderness), internal equipment, and smooth surface roughness; this makes their case worth studying.

This paper focuses on the gust buffeting response in the along- and across-wind directions (also referred to as longitudinal and lateral gust buffeting, respectively) in transcritical Reynolds number regime, starting from the full-scale measurements on a wind turbine tower without rotor-nacelle assembly carried out at Østerild Test Center. The same dataset used by Kurniawati *et al.* (2025) is referred to, and in a way this work represents a completion of the analyses already done on the data. Indeed, this paper aims to clarify the reliability of wind and gust buffeting models proposed by design standards in mild and severe wind conditions. The former represent a typical scenario during crane operations, carried out when the wind velocity at the crane boom is smaller than about 15 m/s (in terms of 10-minute average), and the bolts at the bottom of the tower are partially released or removed to ease the operations, reducing therefore the actual capacity of the system. In this scenario, are gust buffeting load calculations sufficiently accurate, i.e., safe? The latter, instead, refers to survival wind conditions and usually drives the design of the quayside foundation and the grillage of the vessel. Are typical engineering models able to predict the response of the system in ultimate (or survival) design conditions? Although, as discussed above, wind turbine towers prior to the final installation are arranged in groups, this work focuses on the response of an isolated tower and therefore addresses a particular case among the several possibilities. Nevertheless, the isolated tower allows us to avoid the complexity of group interactions and focus more on the modelling of the wind excitation and the structural response.

The remaining part of this work is structured as follows. Section 2 discusses the wind environment through the analysis of full-scale records, with insights on the mean wind profiles, turbulence intensities, integral length scales of turbulence and coherence of the fluctuating velocities. Section 3 presents the dynamic response of the structure with focus on the along- and across-wind gust buffeting, by means of comparisons between the measured full-scale response and calculations with different analytical models. Finally, Section 4 draws some conclusions and perspectives of the work.

## 2. Wind environment

This work focuses on the full-scale measurements got at Østerild Test Center between July 2021 and January 2022, when the Siemens Gamesa 8 MW wind turbine (D8) installed there was without rotor-nacelle assembly. The site is in North-West Denmark (Fig. 1), and this is the area where the prototypes of offshore wind turbines are tested before the serial production.


(a) Location in Europe

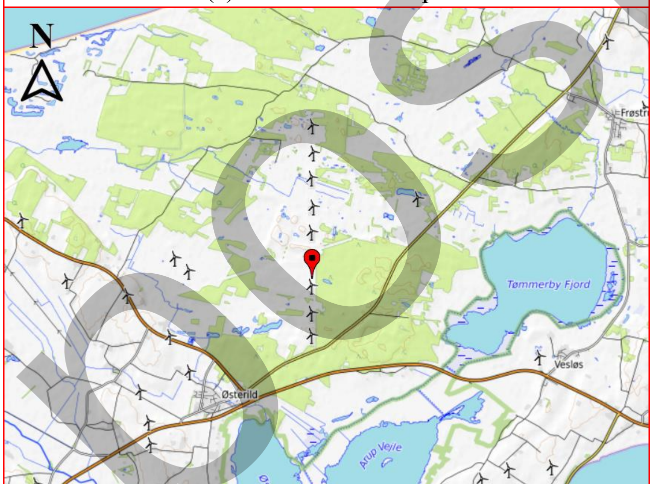


(b) Close-up in Denmark

Fig. 1 Location of Østerild Test Center (source: https://opentopomap.org/).

### *2.1 Measuring system*

The measuring system was designed to have combined measurements of structural response and wind environment (Fig. 2). On the one hand, the response of the tower was measured by strain gauges installed near the bottom flange ($z_m$=18 m) and accelerometers close to the top ($z_a$=109.7 m). On the other hand, wind measurements were taken at multiple heights by two meteorological masts, namely MET 1 and MET 2, nearby the D8 tower, instrumented with sensors able to detect wind velocity and wind direction. Unfortunately, information on temperature, absolute pressure and humidity is available only at one measured height of MET 1 and MET 2 (see Table 1). Accelerations were measured by a three-axes accelerometer produced by Micro-Epsilon (inertial Sensor ACC5703), whereas the strain gauges produced by Micro-Measurements (sensor CEA-06-W250C-350) were used to measure the bending moment. Moreover, the meteorological masts were equipped with Thies cup anemometers (type First Class Advanced) and Thies direction transmitters (type First Class) to measure the horizontal wind velocity and its direction, respectively. All sensors worked with a sampling frequency of 25 Hz.

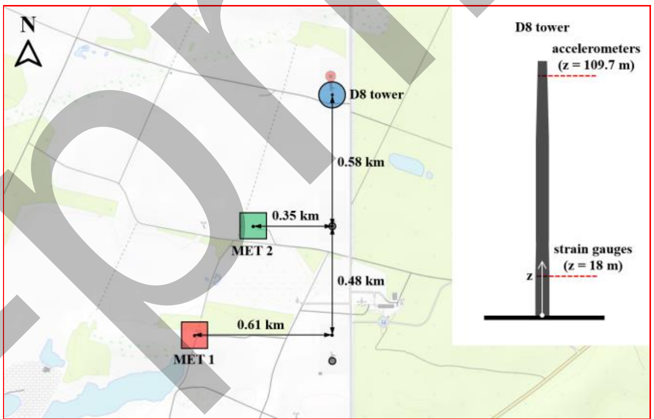


Fig. 2 Layout of the measuring system.

Table 1 Measuring system of the MET masts.

| Mast | *z* [m] | Measurements |
|---|---|---|
| MET 1 | 52 | Wind velocity, wind direction |
| | 87 | Wind velocity |
| | 122 | Wind velocity |
| | 136 | Wind velocity, wind direction, temperature, absolute pressure, humidity |
| | 140 | Wind velocity |
| MET 2 | 49 | Wind velocity, wind direction |
| | 104 | Wind velocity, wind direction |
| | 155 | Temperature, absolute pressure, humidity |
| | 156 | Wind velocity, wind direction |
| | 160 | Wind velocity |

### *2.2 Dataset and preliminary screening*

The dataset used in this study was recorded in four different periods, from July 2021 to January 2022 (see Table 2). In Periods 1, 2 and 3 the wind data are from MET 1, whereas in Period 4 wind data are from MET 2. As detailed by Table 2, not all the sensors were active in the different periods. To identify possible anomalous data and have a general understanding of the magnitude of the records, the maximum moment response in the along- and across-wind directions is preliminary plotted against the corresponding mean wind velocity $v_m$ (Fig. 3, where the velocity at $z$=136 m for Period 4 is calculated based on the power-law regression of available measurements). Further details on how to get the along- and across-wind components of the wind velocity and the response are provided in the following sections. In Period 1, there is an apparent anomalous moment in the along-wind response (point at about 3 MNm for $v_m$(136 m)=7.1 m/s in Fig. 3(a)), most likely due to some activities inside the tower, corresponding to a spike in the acceleration time histories, which cannot be justified at those wind velocities by environmental excitations. Moreover, as is evident from Fig. 3, only Period 4 experienced a satisfying range of wind velocities to have information on both mild and severe wind conditions. For this reason, the results presented in the following sections focus on Period 4 only.

Table 2 Measuring periods analyzed.

| Period | Start | End | Mast | Active sensors, $z$ [m] |
|---|---|---|---|---|
| 1 | 04:10 PM 17.07.2021 | 04:10 PM 27.07.2021 | MET 1 | 52, 87*), 122*), 136, 140*) |
| 2 | 12:00 AM 21.09.2021 | 11:00 PM 25.09.2021 | MET 1 | 87, 122*), 136, 140*) |
| 3 | 12:00 AM 13.10.2021 | 11:00 PM 17.10.2021 | MET 1 | 52, 87*), 136, 140*) |
| 4 | 12:00 AM 27.01.2022 | 10:50 PM 30.01.2022 | MET 2 | 49, 104, 156, 160*) |

Note: Sampling frequency equal to 25 Hz.
*) Wind direction not available.

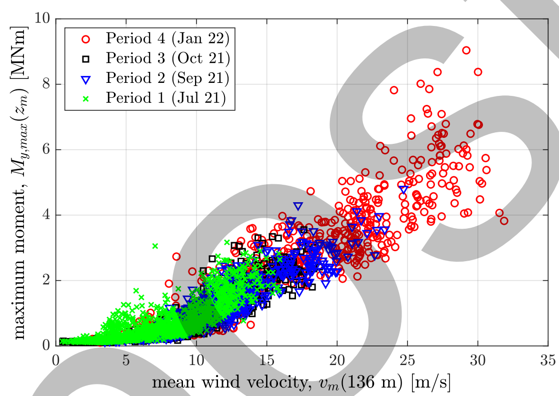


(a) Along-wind

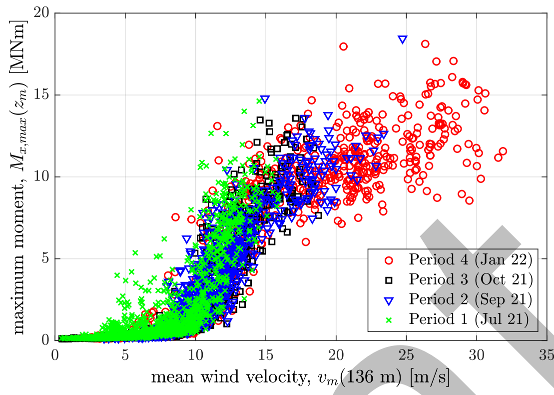


(b) Across-wind

Fig. 3 Structural response (bending moment at $z_m$) during the observation periods.

### 2.3 Reference frames

In the following, let us assume a right-handed Cartesian reference frame $\{O;x,y,z\}$ having the origin $O$ in the geometric center of the base of the tower, $z$-axis pointing vertically upwards and $x$-axis directed along the mean wind direction $\beta$ (Fig. 4). The $y$-axis identifies the across-wind direction. This is the main reference frame used in the post-process of both wind and structural response. Looking at the measuring system, two different reference frames are used, namely: a) the wind velocity is given in a polar frame, by its modulus $v$ and direction $\phi$ (when available) in the wind rose (0 deg corresponds to North and 90 deg corresponds to East); b) the structural response is given in a right-handed Cartesian frame $\{O;\varepsilon,\gamma,z\}$, having the $\varepsilon$-axis rotated by 4 deg in the clockwise direction (i.e., $\theta$=-4 deg) with respect to the North-South direction.

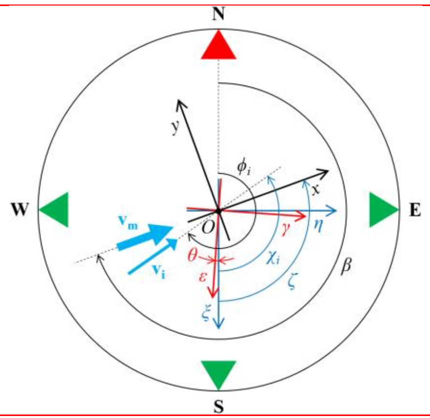


Fig. 4 Reference frames.

### 2.4 Along- and across-wind components

Let us assume an auxiliary (right-handed) reference frame $\{O;\xi,\eta,z\}$, having the $\xi$-axis directed from North to South. Moreover, let us split the time history into $W$ time windows of length $T$. Each window has therefore $N$=$T{\cdot}f_s$ samples, being $f_s$ the sampling frequency. Based on Fig. 4, with focus on the $i$-th sample ($i$=1, 2, …, $N$) of the $k$-th time window ($k$=1, 2, …, $W$), it follows:

$$\chi_i = 2\pi - \phi_i \tag{1}$$

$$v_{\xi,i} = v_i \cdot \cos(\chi_i) \ ; \ v_{\eta,i} = v_i \cdot \sin(\chi_i) \tag{2}$$

$$V_\xi = \frac{1}{N}\sum_{i=1}^{N} v_{\xi,i} \ ; \ V_\eta = \frac{1}{N}\sum_{i=1}^{N} v_{\eta,i} \tag{3}$$

$$v_m = \sqrt{V_\xi^2 + V_\eta^2} \tag{4}$$

$$\zeta = \tan^{-1}\left(\frac{V_\eta}{V_\xi}\right) \tag{5}$$

$$\psi_i = \chi_i - \zeta \tag{6}$$

$$u_{x,i} = v_i \cdot \cos(\psi_i) - v_m \tag{7}$$

$$u_{y,i} = v_i \cdot \sin(\psi_i) \tag{8}$$

where, $v_m$ is the mean wind velocity, while $u_x$ and $u_y$ are the zero-mean turbulent components of the velocity along the $x$- and $y$-axis, respectively. Note that the mean wind direction in the wind rose is $\beta$=–$\zeta$+2$\pi$ rad. In a similar way, it is also possible to identify the along- and across-wind components of the response of the system (see Section 3.5). In the following, the length of the chosen time window is $T$=600 s, and $W$=566 windows are available in Period 4.

### *2.5 Mean wind velocity profile and direction*

The values of the mean wind velocity over 10 minutes of observation are used to estimate the parameters of the wind profile that best fits the data. In the following, a regression of the power-law is used, namely:

$$v_m(z) = v_{ref}\left(\frac{z}{z_{ref}}\right)^{\alpha} \tag{9}$$

where $z_{ref}$ is the reference height, $v_{ref}$ the corresponding mean wind velocity, and $\alpha$ is the exponent of the power-law. The regression, based on the least squares method, of the data got in January from MET 2 (Fig. 5(a)) shows a dispersion of the values of the power-law exponent that is much more pronounced for mean wind velocities smaller than 15 m/s (referred to the top of the tower, i.e., at $h_t$=116.46 m), whereas for relatively high values of the velocity the exponent is approximately in the range 0.2-0.3.

This range of power-law exponent is typical of terrain categories III and IV, as defined by EN 1991-1-4 (e.g., see German and Polish national annexes), which barely match the actual roughness of the area. Indeed, looking at the map of the area (Fig. 1) and referring to a height of more than 100 m, the terrain seems to belong more to category 0 or I for winds coming from the sea ($\beta$ from about 225 deg to 45 deg), and to category II for winds coming from land ($\beta$ in the complementary sector). Clearly, the knowledge of only three values of the velocity along the height, with no values at small elevations where the wind shear is more pronounced, does not allow us to identify a possible shift of the wind profile due to the forest West of Østerild Test Center. However, for the purposes of this paper, the abovementioned power-law regression is considered a sufficiently satisfactory estimation. In this regard, it should also be noted that the characteristics of the mean wind profile next to the ground are of minor importance in the assessment of the tower base bending moment (even more in the present case, where the bending moment is measured at an elevation of 18 m). Moreover, the use of the logarithmic-law profile does not introduce significant improvements in the interpolation of mean wind velocity (Fig. 5(b), where log(•) indicates the natural logarithm of the quantity (•)).

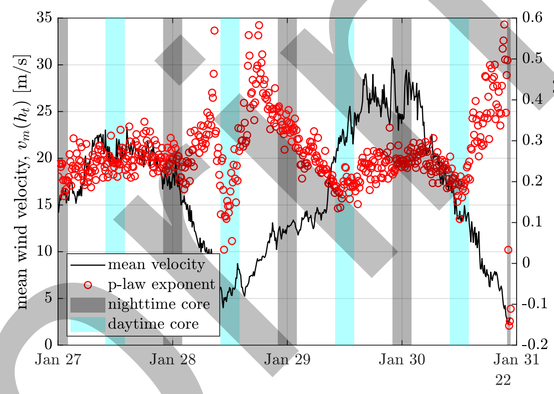


(a) Power-law exponent

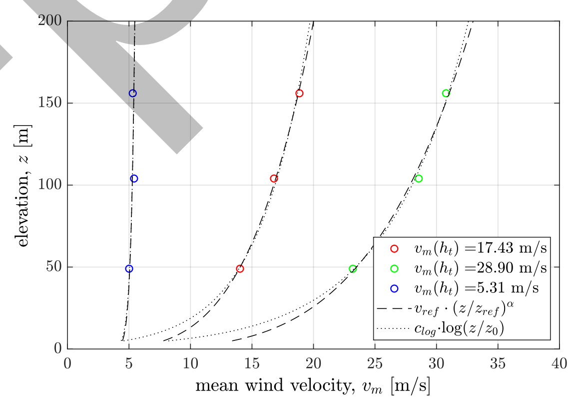


(b) Power law vs. logarithmic law

Fig. 5 Power-law mean wind profile estimated for the data got in Period 4, with $z_{ref}$=10 m and $v_{ref}$ free parameter. Nighttime core from 10 PM to 2 AM, and daytime core from 10 AM to 2 PM.

Focusing on wind velocities at the top of the tower smaller than about 15 m/s, which hereafter are referred to as mild wind conditions, the exponent of the power law clearly indicates that the mean wind profile does not follow the trend typical of neutral atmospheric conditions ($\alpha$ in the range 0.1 to 0.3 in accordance with EN 1991-1-4, German and Polish national annexes). Unfortunately, no comprehensive information about temperature and pressure is available to use more refined models. However, it seems that there are some thermal effects on the mean wind profile, particularly evident following the drop of the power-law exponent around midday. Small variations in the exponent of the power-law profile are also present in the transition from night and day for $v_m(h_t)$>15 m/s, which may still be associated with a less pronounced instability of the atmosphere.

Finally, looking at the mean wind direction in Fig. 6, Period 4 is characterized by winds coming from the sector 210 deg to 330 deg (wind blowing from the North Sea, Fig. 1(a)), with the strongest events in the sector 240 deg to 315 deg.

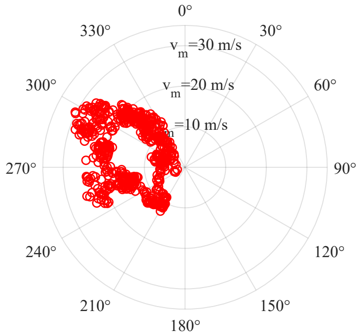


Fig. 6 Mean wind direction $\beta$ at $z$=104 m for the records of Period 4.

### 2.6 Turbulence intensities

The turbulent velocity components of the wind, calculated by means of Eqs. (7)-(8), can be used to estimate the turbulence intensities corresponding to the $W$ time windows, namely:

$$I_{u_x}(z) = \frac{\sigma_{u_x}(z)}{v_m(z)} \; ; \; I_{u_y}(z) = \frac{\sigma_{u_y}(z)}{v_m(z)} \tag{10}$$

where $\sigma_{u_x}$ and $\sigma_{u_y}$ are respectively the standard deviation of the turbulent velocity components in the along- and across-wind directions. Besides few exceptions, particularly evident at extremely low wind velocities (Fig. 7(a)), at $z$=104 m, the turbulence intensity in the $x$-direction $I_{u_x}$ is higher than the turbulence intensity in the $y$-direction $I_{u_y}$, with a ratio of about 0.76 (Fig. 7(b), where the trend line is obtained with a least squares fitting of the first-degree polynomial $y=ax$). Moreover, for mean wind velocities at the top of the tower greater than or equal to 25 m/s, the average value of $I_{u_x}$ ($z$=104 m) is 0.145, whereas the average of $I_{u_y}$ ($z$=104 m) is 0.112. For the sake of comparison, the turbulence intensity of the along-wind component provided by EN 1991-1-4 is 0.096 for terrain category 0, 0.108 for terrain category I, 0.131 for terrain category II, and 0.171 for terrain category III. Therefore, the level of turbulence approximately corresponds to terrain category II.

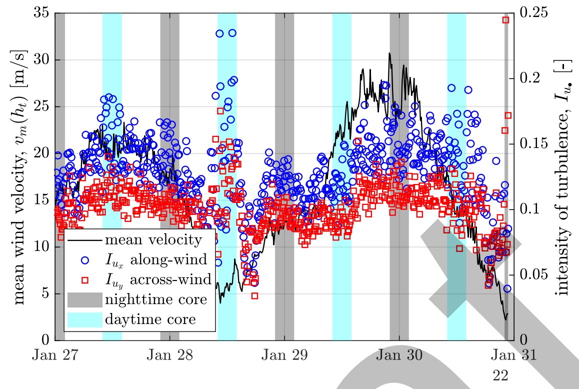


(a) Values across Period 4

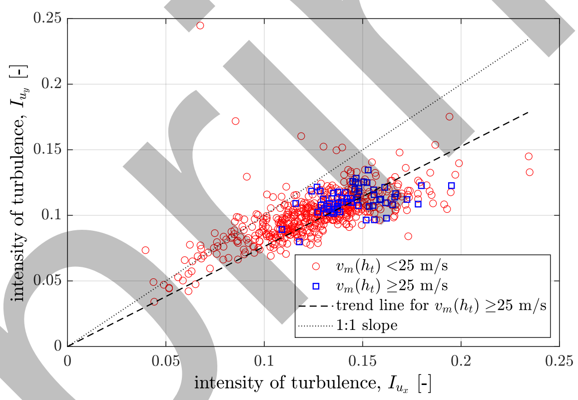


(b) Along- vs. across-wind

Fig. 7 Turbulence intensities at $z$=104 m in the along- and across-wind directions. Nighttime core from 10 PM to 2 AM, and daytime core from 10 AM to 2 PM.

### 2.7 Correlation and integral length scale

The along-wind integral length scale of turbulence $L^x_{u_x}$ is estimated (Fig. 8(a)) in a parametric way with focus on the power spectral density (PSD) of the along-wind turbulent component $S_{u_x}$ to achieve the best fitting between the PSD of measured velocity fluctuations and that given by EN 1991-1-4, namely:

$$\frac{f \cdot S_{u_x}(z,f)}{\sigma^2_{u_x}} = \frac{6.8 \cdot n_x(z,f)}{[1 + 10.2 \cdot n_x(z,f)]^{5/3}} \tag{11}$$

$$n_x(z,f) = \frac{f \cdot L^x_{u_x}(z)}{v_m(z)} \tag{12}$$

Similarly, with focus on the PSD of the across-wind turbulent velocity component $S_{u_y}$, the integral length scale of turbulence of $u_y$, $L^x_{u_y}$, is estimated (Fig. 8(b)) with reference to the PSD given by Solari and Piccardo (2001), namely:

$$\frac{f \cdot S_{u_y}(z,f)}{\sigma^2_{u_y}} = \frac{9.434 \cdot n_y(z,f)}{\left[1 + 14.151 \cdot n_y(z,f)\right]^{5/3}} \tag{13}$$

$$n_y(z,f) = \frac{f \cdot L_{u_y}^x(z)}{v_m(z)} \quad (14)$$

The fittings are carried out considering the nondimensional spectrum and using the nonlinear least squares method; moreover, harmonics beyond 2 Hz are not considered due to the high noise-to-signal ratio. The tendency of the longitudinal integral length scale of turbulence to increase with the mean wind speed is apparent in Fig. 8(a).

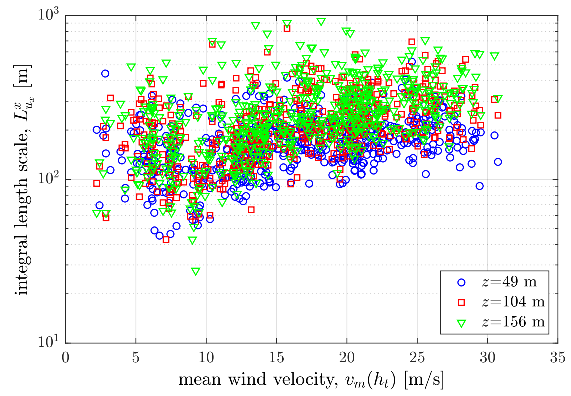


(a) Along-wind

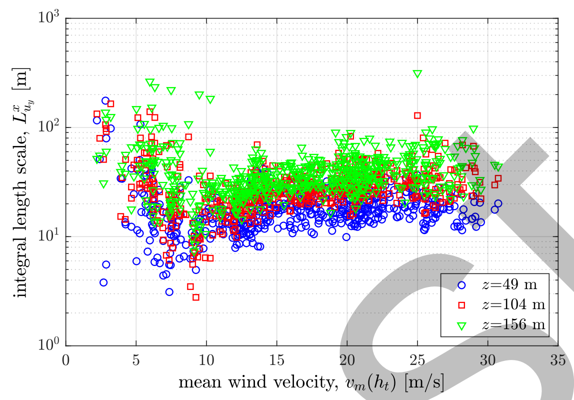


(b) Across-wind

Fig. 8 Integral length scale of turbulence at different heights.

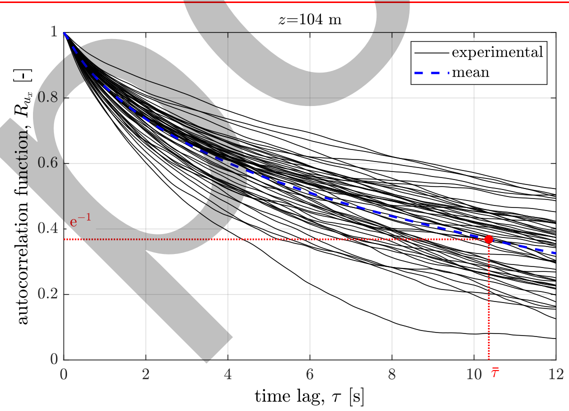


Fig. 9 Example of calculation of the correlation time for an elevation $z$=104 m, limiting to 600 s-time windows characterized by $v_m(h_t)$>25 m/s.

Following a different approach, it is possible to determine the correlation time $\bar{\tau}$ of the along-wind velocity fluctuations, as shown in Fig. 9 (the “exponential fit” technique is used in this case; see, e.g., Teunissen, 1980). Then, relying on Taylor’s frozen eddies hypothesis, the longitudinal integral length scale of turbulence can simply be calculated as (see, e.g., Pope, 2000):

$$L_{u_x}^x = v_m \cdot \bar{\tau} \quad (15)$$

A comparison of the results obtained with this procedure and with the previously mentioned spectral fit is reported in Fig. 10 for the three measurement elevations, limiting to the time windows associated with high mean wind velocities. It is apparent that the correlation function-based estimates fall inside the cloud of values obtained with the spectral fit, close to the mode of the empirical probability density function. For the sake of comparison, the longitudinal integral length scale of turbulence given by EN 1991-1-4 for terrain category II is 213.5 m at $z$=104 m and 144.3 m at $z$=49 m.

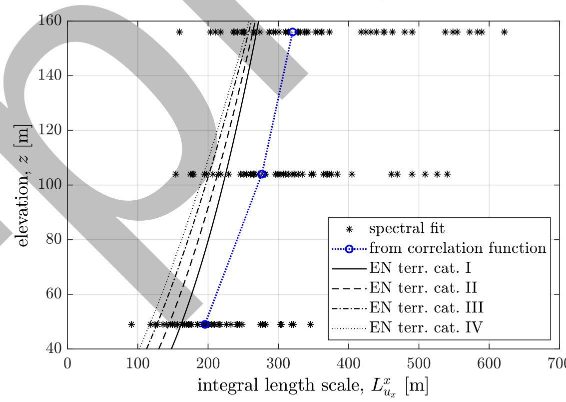


Fig. 10 Comparison of longitudinal integral length scales of turbulence calculated from the correlation function and the spectral fit (limiting to 600 s-time windows characterized by $v_m(h_t)$>25 m/s).

Concerning two-point statistics, the coherence functions of the along- and across-wind turbulent velocity components, respectively $\gamma_{u_x}$ and $\gamma_{u_y}$, are calculated for all point pairs available:

$$\gamma_{u_x}(z_1,z_2,f) = \frac{|S_{u_x}(z_1,z_2,f)|}{\sqrt{S_{u_x}(z_1,f)S_{u_x}(z_2,f)}} \quad (16)$$

$$\gamma_{u_y}(z_1,z_2,f) = \frac{|S_{u_y}(z_1,z_2,f)|}{\sqrt{S_{u_y}(z_1,f)S_{u_y}(z_2,f)}} \quad (17)$$

where $S_{u_x}$ and $S_{u_y}$ denote the spectra (cross-spectra if $z_1 \neq z_2$ and self-spectra if $z_1$=$z_2$) of along- and across-wind velocity components, respectively. Results for the lower pair of points are reported in Fig. 11. No significant differences are observed if co-spectra are used in Eqs. (16)-(17) instead of magnitude of cross-spectra. It is apparent that the coherence does not follow the typical exponential decay suggested by Solari and Piccardo (2001) with the standard decay coefficient in the exponential function equal to 10. In particular, when the frequency tends to zero, the coherence function does not tend to unity (see, e.g., Saranyasoontorn *et al.*, 2004). Moreover, a relatively high level of coherence is found for a wide range of low frequencies (qualitatively similar results are also obtained for the other two pairs of points available from measurements, not reported in Fig. 11 for the sake of brevity). For the along-wind wind velocity component (Fig. 11(a)), Krenk's model (Krenk, 1996; Hansen and Krenk, 1999) is also fitted to the data, using the longitudinal integral length scale of turbulence estimated from the correlation function reported in Fig. 10 (average between the values for the two heights above the ground) and optimizing the decay coefficient in the exponential function. The persistence of coherence for the considered large point distances is somehow captured if a low value of the decay coefficient (around 1) is set. Nevertheless, the coherence for frequencies tending to zero are still overestimated unless an unrealistically low value of the integral length scale of turbulence (in the order of 25 m) is assumed. However, the data available, limited to three points along the height with about 50 m spacing, does not allow a comprehensive understanding of the correlation at closer relative distances (which are important for the dynamic analyses discussed in Section 3) and the implementation of more refined models. For this reason, in the following it is assumed that the wind is correlated in accordance with the model proposed by Solari and Piccardo (2001) and reflected by the prescriptions of EN 1991-1-4, with the remark that this important aspect needs to be further investigated in the future.

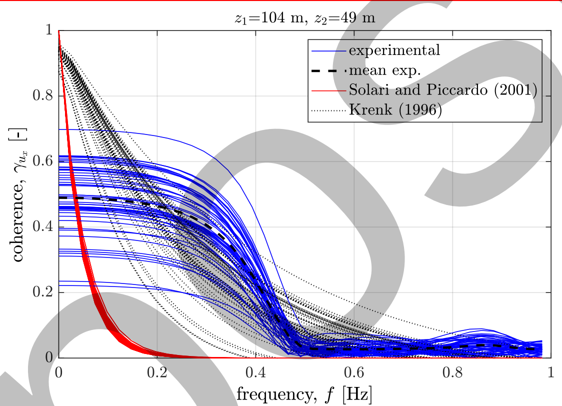


(a) Along-wind

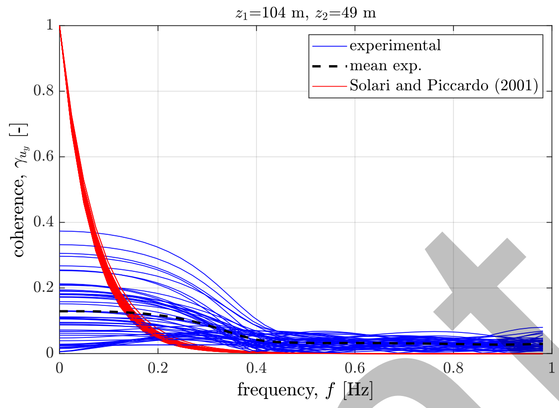


(b) Across-wind

Fig. 11 Coherence function of wind velocity fluctuations at two elevations, limiting to 600 s-time windows characterized by $v_m(h_t)$>25 m/s.

## 3. Structural response

The reference structure of this study, i.e., the D8 tower, is a steel axisymmetric tower with height $h_t$ and annular cross-section, variable in thickness and diameter along the height. The bottom diameter is 6.5 m, and the top diameter is about 4.15 m.

### *3.1 Dynamic properties of the tower*

The records of the response are firstly used to identify the first natural frequency of the system by means of the identification of the first major peak in the PSD of the acceleration under different wind conditions (Fig. 12). The mean value of the first natural frequency $f_1$ is 0.597 Hz, with 5% and 95% fractiles equal to about 0.595 Hz and 0.600 Hz, respectively. The structure can be considered perfectly axisymmetric being a) the first natural frequency along $\varepsilon$-axis equal to the first frequency along the $\gamma$-axis, and b) being isolated the first peak of the spectra. Analogous results can be obtained with a focus on the records of the bending moment. It is noteworthy that this estimation is in perfect agreement with the natural frequency identified for the same wind turbine tower by Mikkelsen *et al.* (2024) by using operational modal analysis, namely 0.595 Hz and 0.596 Hz for the first mode along the two Cartesian axes.

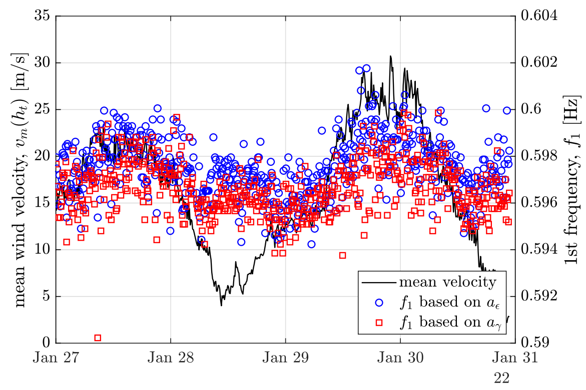


Fig. 12 First natural frequency of the tower evaluated from the records of the acceleration split into 600 s-time windows without overlapping.

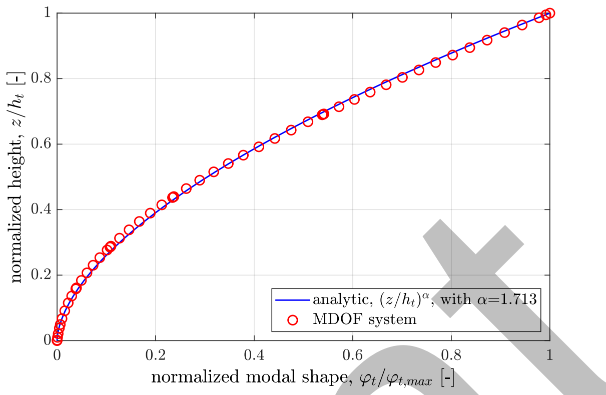


Fig. 14 Analytical form of the first mode shape calculated with the least squares method.

In order to identify the modal shape and modal mass, the tower is modelled as a cantilever beam with an imperfect rotational constraint at the base by using a finite element model based on the Bernoulli-Euler beam element having three degrees of freedom per node, i.e., two translations in the *xz*-plane (or equivalently *yz*-plane, being an axisymmetric system) and the rotation about the *y*-axis (*x*-axis). The rotational stiffness at the base is set to 265 GNm/rad to get the measured first natural frequency (Fig. 13). The first modal shape is almost quadratic, namely well fitted by a power-law with exponent 1.713 (Fig. 14), and the corresponding modal mass $m_{t,1}$ is 100.72 t, evaluated considering the translational degrees of freedom only.

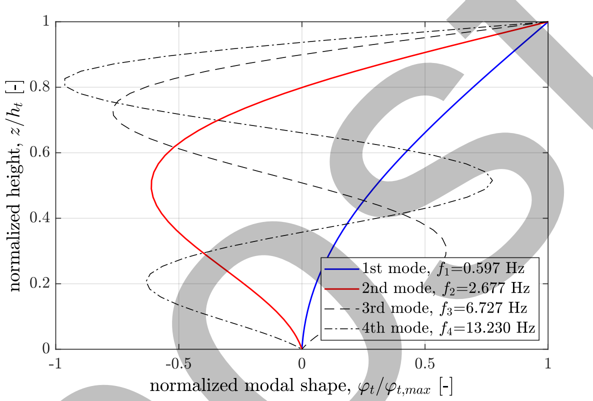


Fig. 13 Mode shapes of the tower calculated with a finite-element model (Bernoulli-Euler beam).

### 3.2 Structural damping

The structural damping of the system is a very uncertain parameter, and it was the subject of a dedicated study via operational modal analysis (Mikkelsen, 2022). Based on the outcomes of that study, it is hereafter assumed a structural damping on the first mode $\delta_s$, also referred to as $\zeta_1$ if given as a ratio of critical damping, in the range 0.19% log. dec. to 2.51% log. dec., or equivalently, 0.03% to 0.4% damping ratio.

### 3.3 Aerodynamic coefficients and damping

The aerodynamic base force $c_f$ and moment $c_m$ coefficients of the tower are assumed equal to 0.594 and 0.622, respectively, based on wind tunnel tests on a similar tower, and they are defined as follows (Barni *et al.*, 2024):

$$c_f = \frac{F_b}{1/2 \cdot \rho_{air} v_m^2(h_t) \int_0^{h_t} D_t(z) dz} \tag{18}$$

$$c_m = \frac{M_b}{1/2 \cdot \rho_{air} v_m^2(h_t) \int_0^{h_t} D_t(z) z\, dz} \tag{19}$$

where $F_b$ is the base shear force, $M_b$ the base bending moment, $\rho_{air}$ the air density and $D_t(z)$ the diameter of the tower along the height. It is noteworthy that the moment coefficient is slightly larger than the force coefficient; this means that the resultant of the aerodynamics forces is applied slightly above the geometric center of the projection of the tower onto a vertical plane. Moreover, these aerodynamic coefficients depend on the mean wind profile, as only the velocity at the top of the tower appears in the normalization of the force and the moment. In the calculations based on the procedure of EN 1991-1-4 (points a) and b) of Section 3.6), the bending moment at $z_m$ is calculated in accordance with the definition of the aerodynamic coefficient $c_m$, given by Eq. (19). By contrast, for the calculation of the aerodynamic damping and in the dynamic approach (see Sections 3.6 and 3.7), a sectional aerodynamic drag coefficient $c_d$ is assumed constant along the height of the tower and equal to the value that, once integrated with the mean velocity pressure profile reproduced in the wind tunnel tests, provides the moment measured at the base of the tower; in this case, $c_d$ is equal to 0.683. This definition implies that the base moment coefficient is not exactly equal to $c_m$, being the wind profile and the tower geometry used in the wind tunnel not exactly the same as the D8 tower at Østerild Test Center; however, the difference is negligible, as it will be discussed in Section 3.8. The aerodynamic damping $\delta_{a,x}$ in the along-wind direction is therefore calculated based on the linearized quasi-steady theory, as follows (in logarithmic decrement):

$$\delta_{a,x} = \frac{\rho_{air} c_d}{2 f_1 m_{t,1}} \int_0^{h_t} D_t(z)\, \varphi_t^2(z) v_m(z) dz \tag{20}$$

where $\varphi_t(z)$ is the first mode shape normalized with respect to the maximum displacement (Fig. 14). Instead, the aerodynamic damping $\delta_{a,y}$ in the across-wind direction is given by:

$$\delta_{a,y} = \frac{\rho_{air} c_d}{4 f_1 m_{t,1}} \int_0^{h_t} D_t(z)\, \varphi_t^2(z) v_m(z) dz \tag{21}$$

### 3.4 Air density

The air density $\rho_{air}$ can be estimated by using the available temperature and atmospheric pressure measurements at $z$=155 m of MET 2. Assuming that the air behaves as an ideal gas, it follows:

$$\rho_{air} = \frac{p}{R T_K} \tag{22}$$

where $p$ is the absolute pressure, $R$ a constant equal to 287 J/(kg·K), and $T_K$ the temperature in Kelvin. The air density in Period 4 ranged from 1.200 kg/m$^3$ to 1.266 kg/m$^3$ (Fig. 15), and it is assumed to be constant along the height of the tower. For the sake of comparison, the air density given by the Danish National Annex to EN 1991-1-4 is 1.25 kg/m$^3$.

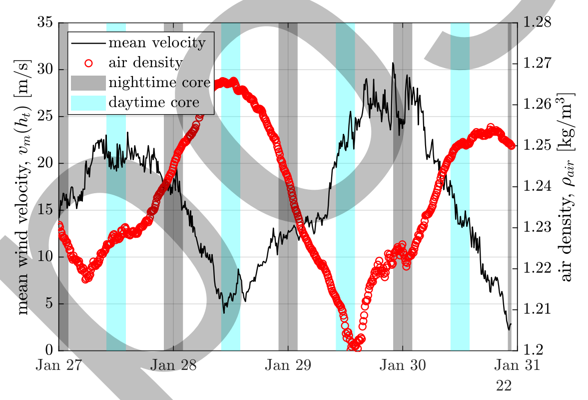


Fig. 15 Air density at $z$=155 m estimated with the ideal gas law. Nighttime core from 10 PM to 2 AM, and daytime core from 10 AM to 2 PM.

### 3.5 Structural response components

The along- and across-wind components of the structural response $r$ can be determined by means of an orthogonal transformation (a rigid rotation) from the reference frame $\{O;\varepsilon,\gamma,z\}$ to $\{O;x,y,z\}$, namely:

$$\kappa = \theta - \zeta \tag{23}$$

$$r_{x,i} = r_{\varepsilon,i} \cdot \cos(\kappa) - r_{\gamma,i} \cdot \sin(\kappa) \tag{24}$$

$$r_{y,i} = r_{\varepsilon,i} \cdot \sin(\kappa) + r_{\gamma,i} \cdot \cos(\kappa) \tag{25}$$

where the response $r$ can be either the bending moment $M$ measured at $z_m$ or the acceleration $a$ measured at $z_a$, hereafter also referred to as acceleration of the top of the tower. Measurements of the bending moment do not allow us to identify the mean component of the internal force, but only the dynamic fluctuations about the mean value. For this reason, in the following the moment $M$ should be regarded as the dynamic part only. On the other hand, the tower displacements $d$ are obtained from the acceleration by using the Fast Fourier Transform (FFT) and its inverse (IFFT), as follows:

$$A_k(f) = FFT[a_k(t)] \text{ with } k = x, y \tag{26}$$

$$D_k(f) = A_k(f)/(j \cdot 2\pi f)^2 \tag{27}$$

$$d_k(t) = IFFT[D_k(f)] \tag{28}$$

where $j$ is the imaginary unit, $f$ the frequency, and $t$ the time. The trajectory of the top of the tower and the power spectral density (PSD) of the displacements are obtained by removing all the harmonics below 0.125 Hz from the spectrum $A$ of the acceleration, so to avoid the spurious contribution of the drift of the accelerometers.

### 3.6 Along-wind response

All the records are split into time windows of $T$=600 s, as done for the wind velocity, and the peak value of the along-wind response (maximum positive value of the response) in each window is extracted and compared with numerical predictions. In particular, the response is calculated in three ways: a) in accordance with the static equivalent procedure given by EN 1991-1-4 as modified by the corresponding Danish National Annex (in particular, please note the use of the Annex C of EN 1991-1-4 for the calculation of the structural factor) for terrain categories I, II, III and IV; b) by using the EN 1991-1-4 procedure mentioned above, but with the inputs measured on site, namely air density, power-law mean wind profile (also reflected in the aerodynamic damping), turbulence intensity, and integral length scale of turbulence; c) following a completely dynamical approach in the frequency domain. Approach c) is based on the strip assumption, that is the drag force per unit length acting on the tower at a certain height above the ground $z$ is assumed to depend just on the wind characteristics at that height. Moreover, the forces are evaluated based on the linearized quasi-steady theory (fluidmemory effects are neglected and the sectional aerodynamic admittance function is assumed to be unity). Finally, assuming Gaussian turbulent fluctuations and projecting the drag force on the first vibration mode (the first vibration mode only is considered here, as it has been verified that the contribution of higher modes to the bending moment is negligible; see also Fig. 22), the following equations are solved:

$$S_{p_1}(f) = \iint_0^{h_t} \Gamma_1(z_1)\Gamma_1(z_2)\gamma_{u_x}(z_1,z_2,f)dz_1dz_2 \tag{29}$$

$$\Gamma_1(z) = \rho_{air} c_d v_m(z) D_t(z) \varphi_{t,1}(z)\sqrt{S_{u_x}(z,f)} \tag{30}$$

$$S_{q_1}(f) = |H_1(f)|^2 S_{p_1}(f) \tag{31}$$

$$|H_1(f)|^2 = \frac{1}{m_{t,1}^2(2\pi f_1)^4}\cdot\frac{1}{\left(1-\frac{f^2}{f_1^2}\right)^2 + 4\zeta_{1,tot}^2\frac{f^2}{f_1^2}} \tag{32}$$

$$\widehat{M}_y = EJ_t(z_m)\cdot|\varphi''_{t,1}(z_m)|\cdot g_{q_1}\cdot\sqrt{\int_0^\infty S_{q_1}(f)df} \tag{33}$$

$$g_{q_1} = \sqrt{2\log(\nu_{q_1,0}^+ T)} + \frac{0.5772}{\sqrt{2\log(\nu_{q_1,0}^+ T)}} \tag{34}$$

$$\nu_{q_1,0}^+ = \frac{1}{2\pi}\sqrt{\frac{\int_0^\infty (2\pi f)^2 S_{q_1}(f)df}{\int_0^\infty S_{q_1}(f)df}} \tag{35}$$

where $S_{p_1}(f)$ indicates the power spectral density of the modal force, $H_1(f)$ is the mechanical admittance function, $\zeta_{1,tot}$ is the critical damping ratio including both structural and aerodynamic damping (Eq. (19)), $S_{q_1}(f)$ is the power spectral density of the response in modal coordinates, $E$ is the Young's modulus of the tower material, $J_t$ is the second moment of area of the tower cross-section, $\widehat{M}_y$ is the peak value of the bending moment at the height $z_m$. $g_{q_1}$ is the peak factor of the modal response based on independent upcrossing theory of stationary random processes, being $\nu_{q_1,0}^+$ the mean zero-upcrossing rate for Gaussian processes and $T$=600 s the observation time. The prime symbol denotes the derivative with respect to $z$. It is worth noting that the peak factor in Eq. (34) is consistent with the way the experimental data are processed, that is extracting only the bending moment maxima and ignoring the minima, in view of the non-negligible mean response of the structure (though not measured) in terms of along-wind bending moment. Moreover, the linearized quasi-steady theory implies a unitary cross-section aerodynamic admittance function.

In the calculations, turbulence intensity and integral length scale of turbulence are interpolated by means of a second-order polynomial regression. This choice allows us to have a good fitting of the three available measurements, but become less reliable, if not wrong, for extrapolations above and below the extreme points. For this reason, below $z$=49 m turbulence intensity and integral length scale are assumed constant and equal to the values at $z$=49 m.

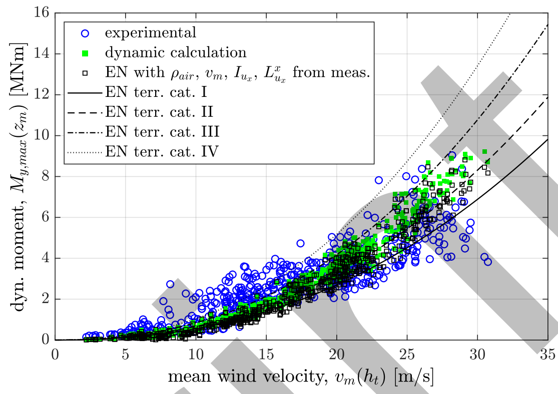


(a) Structural damping $\delta_s$=0.004·2π log. dec.

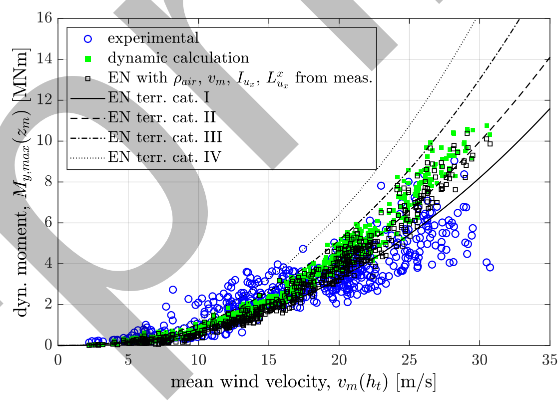


(b) Structural damping $\delta_s$=0.0003·2π log. dec.

Fig. 16 Comparison of the measured along-wind response of the system with the results of different analytical approaches.

As shown in Fig. 16, the models used to estimate the along-wind response exhibit a level of accuracy which depends on the wind velocity range. First, the measured (experimental) bending moment in mild wind conditions ($v_m(h_t)$<15 m/s) tends to be underestimated by all the analytical models. This can be explained by the difficulty of these models to adapt to and describe the peculiarities of the wind environment at low wind velocities. In addition, it is noteworthy that mild wind conditions occur partly in the lock-in range of vortex-induced vibrations, which seems to start at around $v_m(h_t)$=10 m/s (Fig. 3). Even though these conditions are generally not relevant for strength design, they may be important for fatigue design, when combined with the across-wind response. In contrast, during more severe wind conditions, i.e., for wind velocities at the top of the tower greater than about 20 m/s, the capability of the analytical models to correctly predict the measurements strongly depends on the correctness of the wind input parameters, besides the model itself. Generally, all the models tend to better reproduce the measurements if combined with the upper bound of the structural damping. In addition, the methodology proposed by the EN 1991-1-4, modified only using the aerodynamic coefficients from wind tunnel experiments and the aerodynamic damping given by the more general Eq. (20), is very sensitive to the terrain category. Experimental data seems to better fit the trend of low terrain roughness (terrain category I or II), especially at very high wind velocities. In this regard, it is noteworthy that, looking at the turbulence intensity, the area might be associated with a terrain category between I and II, whereas with focus on the wind profile the terrain category is between III and IV. Furthermore, the EN 1991-1-4 procedure combined with the inputs from the measurements, and therefore not directly related to any pre-defined terrain category, shows a trend of the results around terrain category II and very close to the dynamic calculation. The latter, among all the analytical models investigated, is certainly the most consistent method, at the expense of the increased complexity of the calculations, especially for engineering purposes, and the larger number of inputs required. The dynamic calculation (Fig. 17) confirms the tendency of analytical models to underestimate the response in mild wind conditions, whereas for more severe wind velocities the trend is inverted, and it follows the envelope of the upper bound of measured maxima. Similar considerations can be drawn with focus on the standard deviation.

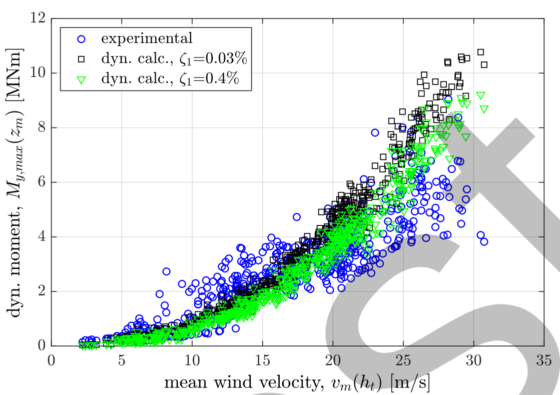


Fig. 17 Comparison of the measured along-wind response of the system with the dynamic calculation of along-wind gust buffeting for different values of damping.

Finally, looking at the skewness $s$ (Fig. 18) and kurtosis $k$ (Fig. 19) of both response and wind velocity fluctuations, it is apparent that these stochastic processes, and in particular those associated with the along-wind response, are not perfectly Gaussian (thus implying $s$=0 and $k$=3), as assumed by the abovementioned analytical models.

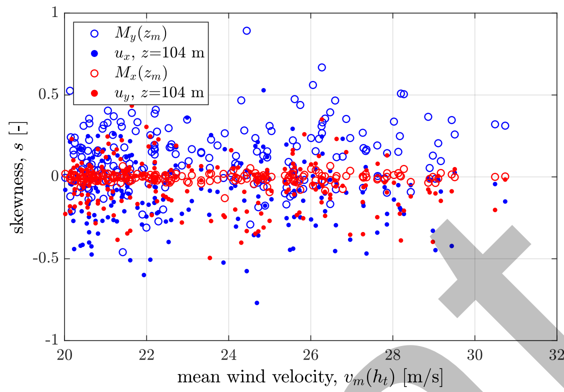


Fig. 18 Skewness of the along- and across-wind components of bending moment response and wind velocity fluctuations for $v_m(h_t)$≥20 m/s.

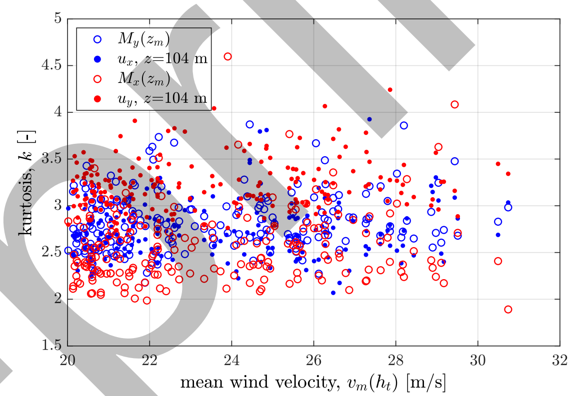


Fig. 19 Kurtosis of the along- and across-wind components of bending moment response and wind velocity fluctuations for $v_m(h_t)$≥20 m/s.

### 3.7 Across-wind response

Similarly to the along-wind case, the $W$ time windows are analyzed focusing on the across-wind gust buffeting response, hereafter also referred to as lateral gust buffeting. By contrast, the response of the tower against vortex shedding was analyzed by Kurniawati *et al.* (2025). The measurements are compared with the response calculated with the same dynamical approach detailed in the previous subsection. Specifically, Eqs. (29)-(30) are replaced by:

$$\tilde{S}_{p_1}(f) = \iint_0^{h_t} \tilde{\Gamma}_1(z_1)\tilde{\Gamma}_1(z_2)\gamma_{u_y}(z_1,z_2,f)dz_1dz_2 \tag{36}$$

$$\tilde{\Gamma}_1(z) = \frac{1}{2}\rho_{air}c_d v_m(z)D_t(z)\varphi_{t,1}(z)\sqrt{S_{u_y}(z,f)} \tag{37}$$

Moreover, the mechanical admittance function $H_1(f)$ incorporates the across-wind aerodynamic damping (Eq. (21)), and the peak factor reads:

$$g_{q_1} = \sqrt{2\log\left(2v^+_{q_1,0}T\right)} + \frac{0.5772}{\sqrt{2\log\left(2v^+_{q_1,0}T\right)}} \tag{38}$$

to account for the fact that in the across-wind direction the mean response is null, and maxima and minima are equally important (consistently with the postprocess of the measurements). In addition, the analytical gust buffeting model proposed by CNR- DT 207 R1/2018, combined with the mean wind velocity profile, turbulence intensity and integral length scale of turbulence from EN 1991-1-4, is also considered.

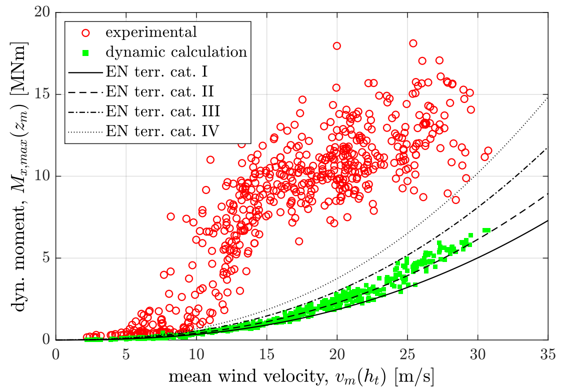


(a) Structural damping $\delta_s$=0.004·2π log. dec.

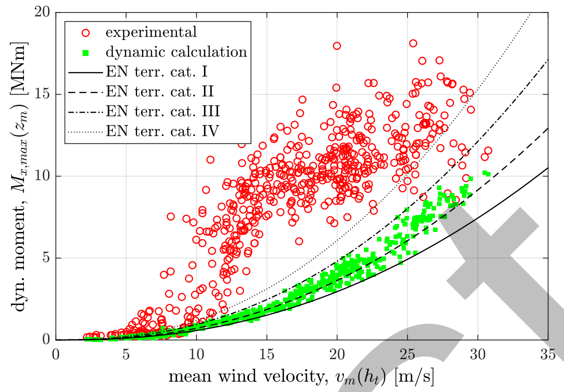


(b) Structural damping $\delta_s$=0.0003·2π log. dec.

Fig. 20 Comparison of the measured across-wind response of the system with the results of the analytical model from the Recommendations CNR-DT 207 R1/2018, using wind inputs from EN 1991-1-4.

As shown in Fig. 20, with focus on wind velocities at the top of the tower larger than 25 m/s, which are referred to as post lock-in regime in Kurniawati *et al.* (2025), the dynamic response of the tower is not well reproduced by analytical gust buffeting models, even for low values of structural damping. The dynamic gust buffeting calculation (Fig. 21) corroborates the observed tendency of analytical models to underestimate the response. The gap is even larger in terms of standard deviation of the response, highlighting a lower peak factor in the measured response compared to the analytical model. This difficulty in reproducing the across-wind response as a pure gust buffeting event should be further investigated, starting from a better understanding of all characteristics of the wind environment and how it may affect the response.

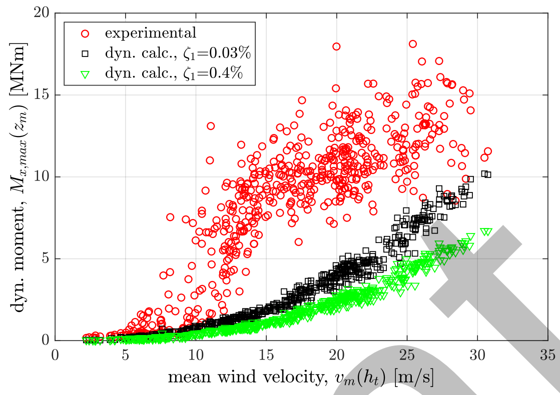


Fig. 21 Comparison of the measured across-wind response of the system with the dynamic calculation of lateral gust buffeting for different values of damping.

### *3.8 Further discussion of the results*

In the previous sections, the inadequacy of models from EN 1991-1-4 in capturing the features of mild wind conditions is discussed. This is apparent both in the description of the wind environment and in the estimation of the along-wind gust buffeting response, which does not follow the envelope of experimental data. In contrast, for $v_m(h_t)$>25 m/s the measurements show better agreement with the models of EN 1991-1-4, although there are some discrepancies. In particular, a) the mean wind profile and turbulence intensity correspond to different terrain categories, namely (on average) above category III and slightly above category II, respectively; b) the longitudinal integral length scale of turbulence tends to be underestimated by the model of EN 1991-1-4; c) the coherence of the low-frequency velocity fluctuations associated with the background response of the tower is higher than predicted by the model behind EN 1991-1-4 (except for very low frequency components), although more important information on closely spaced points is missed. Among these factors, the turbulence intensity seems to be the parameter that most influences the response, also given that the mean wind velocity profile in the lower part of the tower does not significantly affect its dynamic behavior. This is confirmed by the dynamic calculations, which follow indeed the terrain category representative of turbulence intensity. On the other hand, the across-wind response significantly deviates from predictions based on lateral gust buffeting calculations.

To better inspect the comparison between the measured and calculated response and to understand the reasons for the discrepancies in the across-wind moment, their PSDs are compared, as shown in Fig. 22. Despite all the uncertainties, the background response is well captured by the dynamic calculation (even for the across-wind response, although the quasi-static contribution is only marginal in that case). Moreover, the results for the along-wind response (Fig. 22(a)) seem to be consistent with a damping ratio intermediate between the minimum and maximum values identified (0.03% and 0.4%, respectively). In contrast, the dynamic calculations underestimate the measured across-wind response due to the high and very wide resonant peak (Fig. 22(b)). This feature of the response spectrum is not consistent with the linear behavior of the system and highlights the presence of additional nonlinear aeroelastic effects, also relevant at high wind velocities. Finally, it is apparent that, consistently with full-scale measurements, the contribution of the second vibration mode is negligible for both the along- and across-wind response.

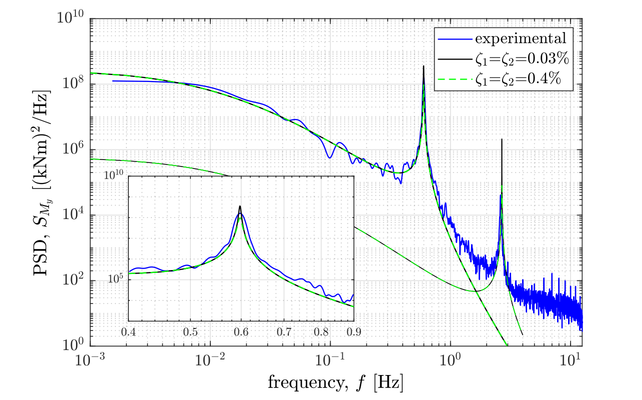


(a) Along-wind

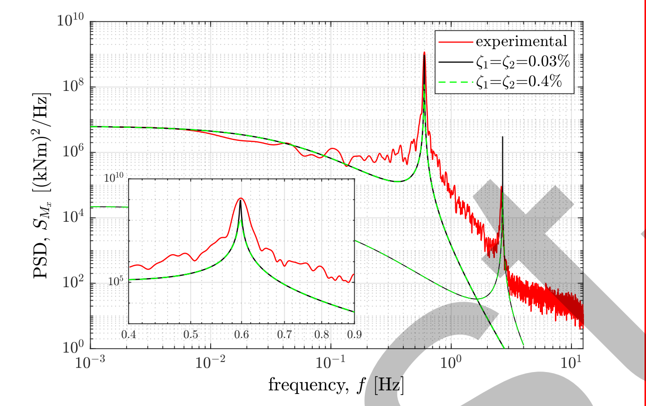


(b) Across-wind

Fig. 22 Comparison of the power spectral density (PSD) of the measured response of the system with the PSD given by the dynamic calculation. A close-up view of the resonant peak is reported in the internal frame of the figure. Time window with $v_m(h_t)$=24.9 m/s.

In addition, besides the results presented in the previous sections, each of the $W$ time windows is analyzed in much more detail to investigate all the main aspects of wind-structure interaction, from the characterization of the wind environment to the analysis of the response. Fig. 23 shows a summary of the main quantities for a time window with mean wind velocity falling in the lock-in range of vortex-induced vibrations ($v_m(h_t)$=17.4 m/s), where the across-wind response is dominant, as can immediately be seen from the trajectory (top-left panel). The wind profile is well fitted by a power law with $\alpha$=0.256 (top-center panel), and the turbulence intensities in the along- and across-wind directions have a ratio of about 0.93 (top-right panel), with an along-wind value at $z$=104 m of 12.5%. Although the exponent of the mean wind velocity profile is close to the terrain category III of EN 1991-1-4, the turbulence intensity is instead close to the value of terrain category II, i.e., 13.1%. Looking at the PSDs, along-wind wind velocity fluctuations are in good agreement with the analytical spectrum given by EN 1991-1-4, and the deviation from the –5/3 slope is just pronounced at high frequencies (bottom-left panel). The top displacement shows a first peak corresponding to the identified first natural frequency, and the standard deviation highlights a dominant motion in the across-wind direction (bottom-center panel); in a similar way, this also occurs for the PSD of the components of bending moment and their standard deviation (bottom-right panel). Fig. 24 shows the analysis of a time window during a severe wind condition ($v_m(h_t)$=28.9 m/s). In this case the trajectory has a more pronounced along-wind component, and the along- and across-wind turbulence intensities have a ratio of about 0.82. Moreover, the PSDs of the velocity fluctuations better match the spectrum of EN 1991-1-4. By contrast, in case of mild wind conditions, as shown in Fig. 25, the trajectory become more chaotic, the turbulence intensity in the along- and across-wind direction may not respect anymore the typical ratios ($y$-direction can be even more turbulent than the $x$-direction), and the PSD of the wind velocity fluctuations does not exhibit the classical slope of –5/3. This highlights again the well-known inadequacy of the models to properly represent mild wind conditions.

Despite the effort put into modelling the different factors with the highest possible fidelity, there are still some uncertainties that should be addressed in the future with additional tests, namely: a) the coherence function seems not to follow the classical exponential decay (unfortunately, only measurement at few heights are available); it would be important to further investigate this aspect and the effects on gust buffeting loads (it is known that the latter can be more correlated than wind field); b) the aerodynamic coefficients are identified by an educated estimation based on wind tunnel tests on similar structures; however, the D8 tower was not specifically investigated in the wind tunnel neither in terms of actual geometry nor in terms of local wind environment; c) the structural damping needs to be better clarified, even though the available estimations through operational modal analysis allowed us to identify a possible range.

Finally, a note about the use of the aerodynamic moment $c_m$ and drag $c_d$ coefficients for the calculation of the bending moment at the height of the strain gauges. In this work two different approaches are used: a) the EN 1991-1-4 procedure with focus on a global aerodynamic coefficient $c_m$ defined by Eq. (19); b) the dynamical gust buffeting calculation with reference to a sectional force coefficient, $c_d$. Is the choice of these coefficients consistent? Let us consider the following two integrals reflecting a calculation of the bending moment at $z_m$ in accordance with EN 1991-1-4 with the two different aerodynamic coefficients (net of the shared constants), namely:

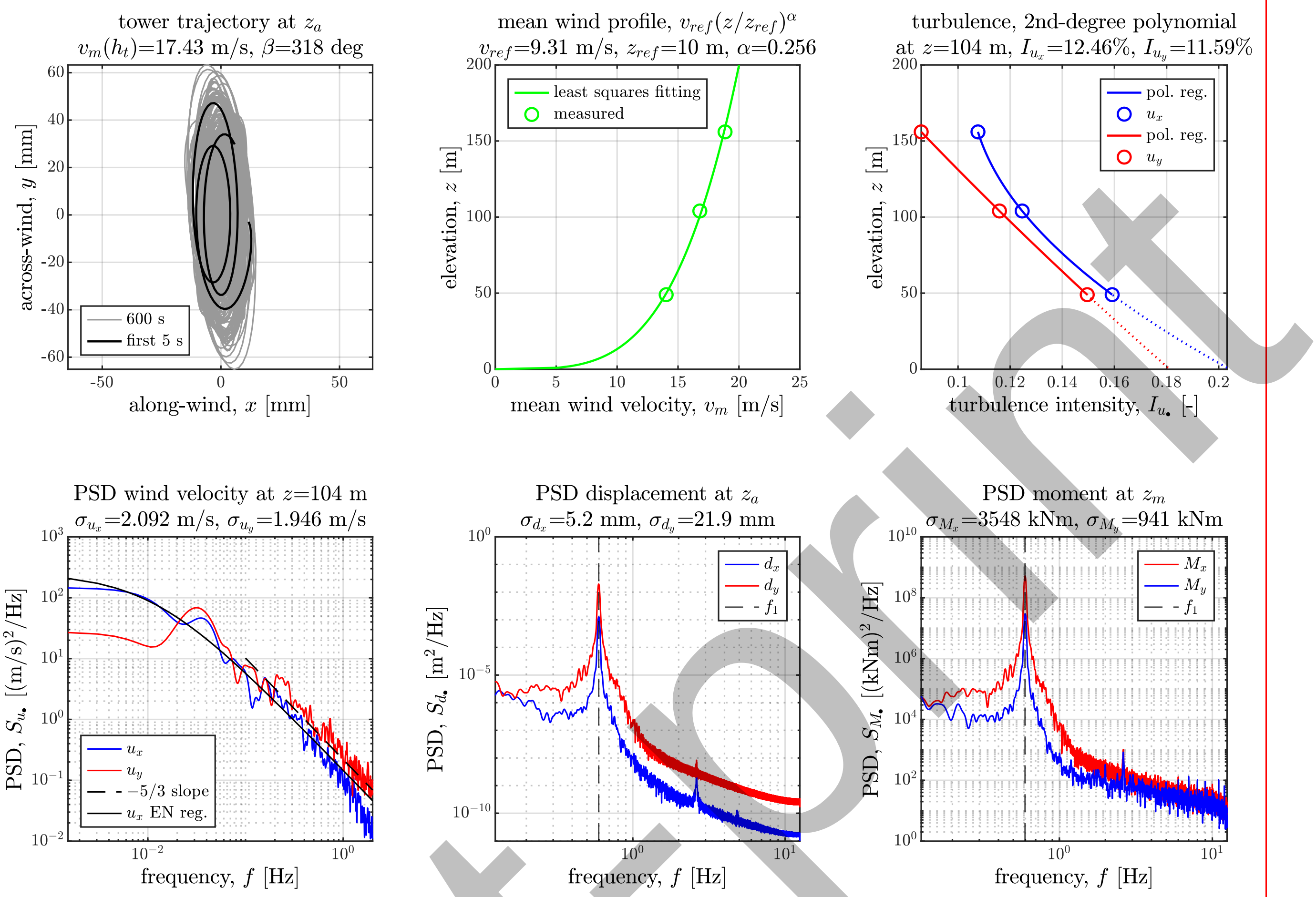


Fig. 23 Summary of the main features of the wind environment and response of the tower during an event in the lock-in range of wind-induced vibrations.

$$B_1 = c_m q_m^*(h_t)[1 + 7I(h_t)] \int_{z_m}^{h_t} D_t(z)(z - z_m)\, dz \quad (39)$$

$$B_2 = c_d \int_{z_m}^{h_t} q_m^*(z)[1 + 7I(z)] \cdot D_t(z)(z - z_m)\, dz \quad (40)$$

$$q_m^*(z) = \left[\log\left(\frac{z}{z_0}\right)\right]^2 \;;\; I(z) = \frac{1}{\log(z/z_0)} \quad (41)$$

where $q_m^*$ is a pseudo-mean velocity pressure, net of the terms that do not depend on $z$, and $z_0$ is the roughness length. The ratio $B_1/B_2$ for $z_0$ in the range from 0.003 m to 1.0 m is close to unity, ranging from 0.97 to 1.03, proving the equivalence of the two approaches with the selected aerodynamic coefficients.

## 4. Conclusions and perspectives

The present work discussed the accuracy of gust buffeting models underlying common design standards in predicting the response of a wind turbine tower without rotor-nacelle assembly in mild and severe wind conditions, through the analysis of combined full-scale measurements of wind and structural response. The main takeaways of this work can be summarized as follows:

- **Wind environment**. The formulations provided by design standards for mean wind profiles, turbulence intensity and turbulence spectra can well reproduce the wind measurements at high wind velocities with reasonable values of model parameters. By contrast, at low wind velocities the same models have an apparent difficulty in reproducing the actual conditions, as the atmospheric neutral conditions of stability are not met anymore. In addition, the integral length scale of turbulence, calculated in a parametric way, presents a broad range of values and tends to be higher than the prescriptions of EN 1991-1-4. Finally, the coherence evaluated with experimental data does not follow the exponential models underlying EN 1991-1-4, at least for relatively large point distances. This aspect should be further investigated by measurements at smaller relative distances.

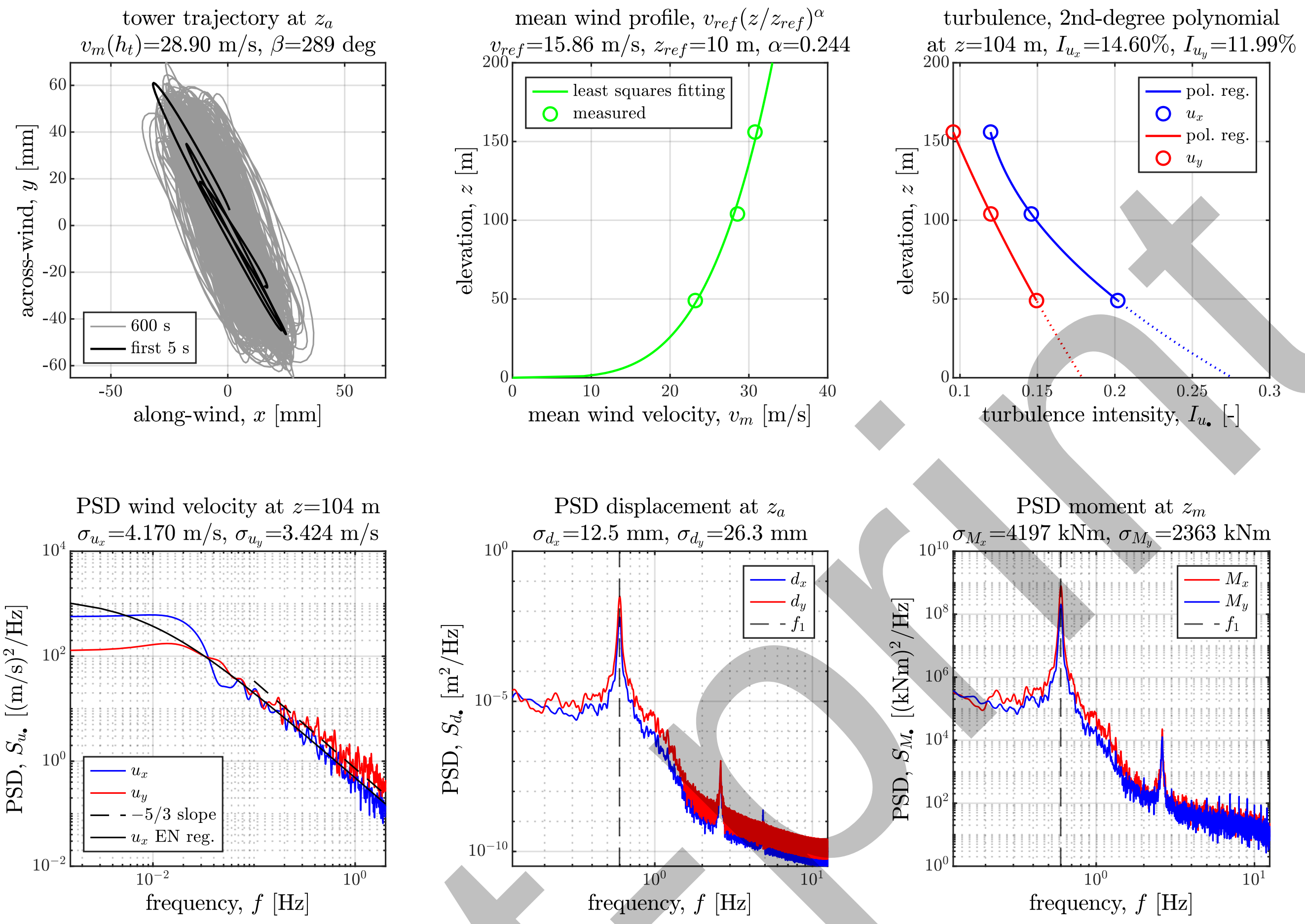


Fig. 24 Summary of the main features of the wind environment and response of the tower during a severe wind velocity event.

- **Along-wind response**. The analytical models are in good agreement with the measurements, especially at relatively high wind velocities and for the upper bound of the estimated structural damping. Experimental data are generally more scattered than analytical calculations, probably due to specific features of the wind not completely captured by the models. Moreover, the measurements tend to be slightly overestimated by calculations at high wind velocities, and, conversely, underestimated in mild wind conditions, with all the limitations of the representativeness of the models in those conditions. Finally, the dynamic gust buffeting calculations proposed in this work, with few exceptions, can reasonably capture the background of the measured along-wind response as well as the resonant peak.
- **Across-wind response**. The large value of the measured response at high wind velocities, i.e., beyond the expected range of vortex-induced vibrations, cannot be justified by a pure lateral gust buffeting response, and this is valid regardless of the structural damping value assumed. Moreover, the energy associated with the resonant spectral peak in the measurements is not compatible with the results of gust buffeting dynamic calculations. This highlights the presence of additional nonlinear aeroelastic effects. Further investigations are needed into this important point, and they would require a better characterization of the actual wind environment, including a more reliable evaluation of wind coherence.

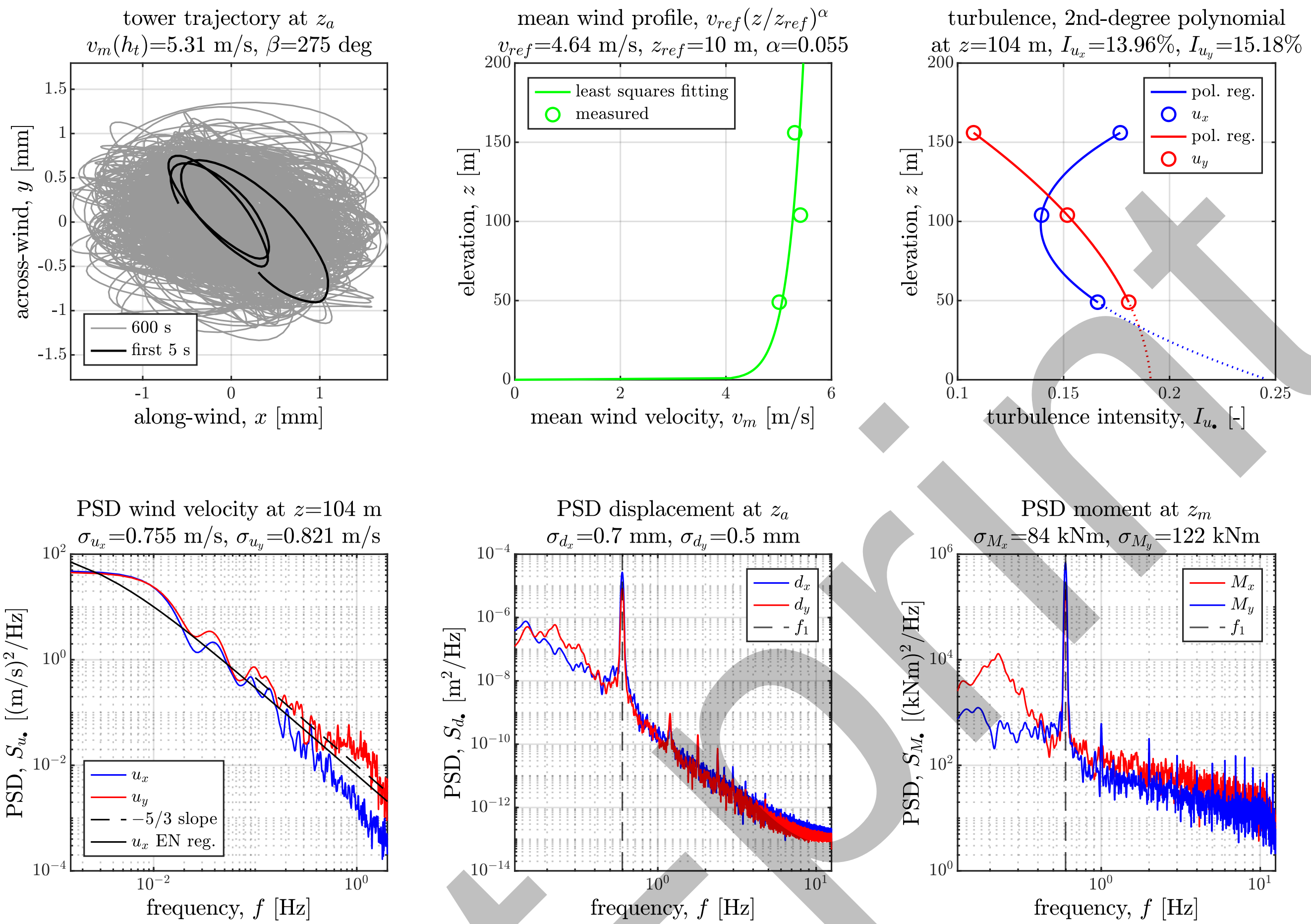


Fig. 25 Summary of the main features of the wind environment and response of the tower during mild wind velocity conditions.

## References


Barni, N., Bartoli, G., Mannini, C. and Massai, T. (2024), "Wind tunnel tests for the experimental assessment of aerodynamic coefficients of 140 m-high towers arranged in groups", Report: Siemens-03/24, CRIACIV-DICEA, University of Florence, Italy.

Cheng, C-M. and Kareem, A. (1992), "Acrosswind response of reinforced concrete chimneys", *Journal of Wind Engineering and Industrial Aerodynamics*, **43**(1), 2141-2152.

Christensen, O. and Askegaard, V. (1978), "Wind forces on and excitation of a 130-m concrete chimney", *Journal of Wind Engineering and Industrial Aerodynamics*, **3**(1), 61-77.

CNR-DT 207 R1/2018 (2019), "Istruzioni per la valutazione delle azioni e degli effetti del vento sulle costruzioni", National Research Council of Italy (in Italian).

DIN EN 1991-1-4/NA (2010), "National Annex to Eurocode 1: Actions on structures – Part 1-4: General actions – Wind actions", Deutsches Institut für Normung (DIN).

DS/EN 1991-1-4 DK NA (2015), "National Annex to Eurocode 1: Actions on structures – Part 1-4: General actions – Wind actions", Danish Standards Foundation.

Ellingsen, Ø.M., Flamand, O., Amandolese, X., Coiffet, F., and Hémon, P. (2021), "Field Tests on a Full-Scale Steel Chimney Subjected to Vortex-Induced Vibrations", *Structural Engineering International*, **32**(1), 55–61.

EN 1991-1-4 (2005), "Eurocode 1: Actions on structures – Part 1-4: General actions – Wind actions", European Committee for Standardization.

EN 1991-1-6 (2005), "Eurocode 1: Actions on structures – Part 1-6: General actions – Actions during execution", European Committee for Standardization.

Esteban, M.D., Diez, J.J., López, J.S. and Negro, V. (2011), "Why offshore wind energy?", *Renewable Energy*, **36**, 444-450.

Galemann, T. and Ruscheweyh, H. (1992), "Measurements of wind induced vibrations of a full-scale steel chimney", *Journal of Wind Engineering and Industrial Aerodynamics*, **41**(1), 241-252.

Hansen, S.O. (1981), "Cross-wind vibrations of a 130-m tapered concrete chimney", *Journal of Wind Engineering and Industrial Aerodynamics*, **8**(1), 145-155.

Hansen, S.O. and Krenk, S. (1999), "Dynamic along-wind response of simple structures", *Journal of Wind Engineering and Industrial Aerodynamics*, **82**(1-3), 147-171.

Hirsch, G. and Ruscheweyh, H. (1975), "Full-scale measurements on steel chimney stacks", *Journal of Wind Engineering and Industrial Aerodynamics*, **1**, 341-347.

Krenk, S. (1996), "Wind field coherence and dynamic wind forces", In: Naess, A. and Krenk, S. (eds), *Advances in Nonlinear Stochastic Mechanics, Volume 47 (SMIA),* pp. 269-278. Proceedings of the IUTAM Symposium on Advances in Nonlinear Stochastic Mechanics, Springer, Kluwer, Dordrecht.

Kurniawati, I., Lupi, F., Seidel, M., Niemann, H.-J. and Höffer, R.

(2024), “Vortex shedding load on a full-scale wind turbine tower at transcritical Reynolds numbers”, *Journal of Wind Engineering and Industrial Aerodynamics*, **252**, 105821.

Kurniawati, I., Lupi, F., Seidel, M., Höffer, R. and Niemann, H.-J. (2025), “Vortex-induced vibrations and post-lock-in cross-wind oscillations of wind turbine tower based on field measurements”, *Journal of Wind Engineering and Industrial Aerodynamics*, **258**, 106010.

Manal, Y. and Hémon, P. (2024), “Unsteady loads on circular cylinder in cross-flow: An observation in natural wind and comparison with wind tunnel experiments*”, Journal of Fluids and Structures*, **124**, 104019.

Mannini, C., Massai, T., Giachetti, A. and Giusti, A. (2023), “Aerodynamic loads on groups of offshore wind turbine towers stored on quaysides during the pre-assembly phase”, *Journal of Wind Engineering and Industrial Aerodynamics*, **242**, 105569.

Mannini, C., Massai, T., Giachetti, A. and Giusti, A. (2024), “Aerodynamic loads on wind turbine towers arranged in groups with and without helical strakes”, *Proceedings of the XVII Conference of the Italian Association for Wind Engineering – IN-VENTO 2022*, Milan, Italy.

Mannini, C., Massai, T., Giachetti, A. and Giusti, A. (2026), “Dynamic loading of offshore wind turbine towers arranged in groups on port quaysides”, *Proceedings of the 16th International Conference on Wind Engineering – ICWE16*, Florence, Italy (in press).

Melbourne, W.H., Cheung, J.C.K. and Goddard, C.R. (1983), “Response to wind action of 265-m Mount Isa Stack”, *Journal of Structural Engineering*, **109**(11), 2561-2577.

Mikkelsen, J.K. (2022), “Comparison of modal parameters of a wind turbine by Operational Modal Analysis and a Finite Element Method”, MSc. Thesis, University of Southern Denmark - Faculty of Engineering.

Mikkelsen, J.K., Orlowitz, E. and Juhl, P.M. (2024), “Automated operational modal analysis on a full-scale wind turbine tower”, In: Dilworth, B.J., Marinone, T. and Mains, M. (eds), *Topics in Modal Analysis & Parameter Identification, Volume 9*. SEM 2023. Conference Proceedings of the Society for Experimental Mechanics Series, Springer, Cham.

Müller, F.P. and Nieser, H. (1975), “Measurements of wind-induced vibrations on a concrete chimney”, *Journal of Wind Engineering and Industrial Aerodynamics*, **1**, 239-248.

PN-EN 1991-1-4/NA (2010), “National Annex to Eurocode 1: Actions on structures – Part 1-4: General actions – Wind actions”, Polskiego Komitetu Normalizacyjnego (PKN).

Pope, S.B. (2000), *Turbulent Flows*, Cambridge University Press, Cambridge, UK.

Sanada, S., Suzuki, M. and Matsumoto, H. (1992), “Full scale measurements of wind force acting on a 200m concrete chimney, and the chimney’s response”, *Journal of Wind Engineering and Industrial Aerodynamics*, **43**(1), 2165-2176.

Saranyasoontorn, K., Manuel, L. and Veers, P.S. (2004), “A comparison of standard coherence models for inflow turbulence with estimates from field measurements”, *Journal of Solar Energy Engineering*, **126**(4), 1069-1082.

Solari, G. and Piccardo, G. (2001), “Probabilistic 3-D turbulence modeling for gust buffeting of structures”, *Probabilistic Engineering Mechanics*, **16**(1), 73-86.

Teunissen, H.W. (1980), “Structure of mean winds and turbulence in the planetary boundary layer over rural terrain”, *Boundary-Layer Metheorology*, **19**, 187-221.

Waldeck, J.L. (1992), “The measured and predicted response of a 300 m concrete chimney”, *Journal of Wind Engineering and Industrial Aerodynamics*, **41**(1), 229-240.